Kovove Mater. 62 2024 77–90
DOI: 10.31577/km.2024.2.77

The impact of shielding gas composition and welding speed on weld quality in MAG welding: An experimental study

Esin Tuğba Şimşek Çelik[1]*, Ahmet Akkuş[2]

[1]*Sivas Cumhuriyet University, Hafik Kamer Ornek Vocational School of Higher Education, Department of Transportation Services, Rail Systems Management Program, Sivas, Turkey*
[2]*Sivas Cumhuriyet University, Engineering Faculty, Mechanical Engineering Department, Sivas, Turkey*

Received 27 December 2023, received in revised form 28 February 2024, accepted 26 March 2024

Abstract

This study aimed to investigate the impact of various shielding gas compositions and welding speeds on the welding quality of S355J2 with normalized structural steel, which was welded using the semi-automatic MAG (Metal Active Gas) welding method. To achieve this, a total of 27 welded parts were produced using 9 different gas mixtures and 3 different welding speeds, and the welding quality was observed and analyzed. Hardness test, bending test, optical microscope, SEM (Scanning Electron Microscope), and EDS (Energy Dispersive Spectrometry) examinations of the samples obtained from the welded parts were carried out.

This study shows that as the welding speed increases, the heat input of the weld decreases, and thus, the cooling rate of the HAZ (Heat Affected Zone) increases, which increases the weld metal hardness. The hardness of the weld metal decreases as the amount of carbon dioxide increases, which increases heat input and, thus, cooling time.

K e y w o r d s: MAG welding, metal active gas welding, S355 structural steel, shielding gas composition, automatic welding

1. Introduction

Due to its economical and practical nature, the MIG-MAG (Gas Metal Arc Welding) method is widely used in machinery manufacturing, transportation, and the mining industry. This method allows for uninterrupted welding and control of welding parameters and is suitable for automation [1, 2]. Metal Active Gas (MAG) welding can be done manually or fully automatically, as it is an arc welding method with an endless and melting wire electrode under a protective gas atmosphere [3].

In the welding process, the gases protect the droplets, weld pool, and heat-affected area from the surrounding air while also enhancing the behavior of the welding arc. Shielding gases commonly used for welding steels include pure argon, mixtures of argon and carbon dioxide, mixtures of argon and oxygen, mixtures of argon + carbon dioxide + oxygen, and pure carbon dioxide gas [4–7].

Structural steel is used in various fields, including bridges, railways, shipbuilding, and offshore oil and gas exploration platforms. The MIG/MAG welding method is widely used to join structural steels, and research is also being conducted to improve the shielding gases used in this process [8].

In a study by Türk & Demirer [9], an overlay was created by combining surface-hardened S355J0 structural steel with unhardened structural steel of the same quality using two different shielding gas mixtures (88 % argon + 10 % carbon dioxide + 2 % oxygen and 100 % carbon dioxide) through the MAG welding method. The influence of shielding gas and bevel treatment on the mechanical properties and the shape of the weld seam geometry was examined. Avisans et al. [10] examined the impact of an 8 % carbon dioxide blend in argon on MAG welding of low alloy high-strength steel at high welding parameters. The combination of lower welding parameters resulted in superior penetration, inclusion, and hardness outcomes. Kargın et al. [11] conducted MAG welding of S460MC steel plates using two different welding

*Corresponding author: e-mail address: esimsek@cumhuriyet.edu.tr

Table 1. Chemical composition (wt.%) of S355J2 with normalized structural steel

C	Mn	P	Si	Cu	N	S	Al	B	V	Ti	Nb	Cr	Ni	Mo	As	Sn
0.1758	1.431	0.0105	0.0092	0.0186	0.0071	0.0056	0.0365	0.0001	0.0024	0.0011	0.0040	0.0192	0.0295	0.0020	0.0007	0.0015

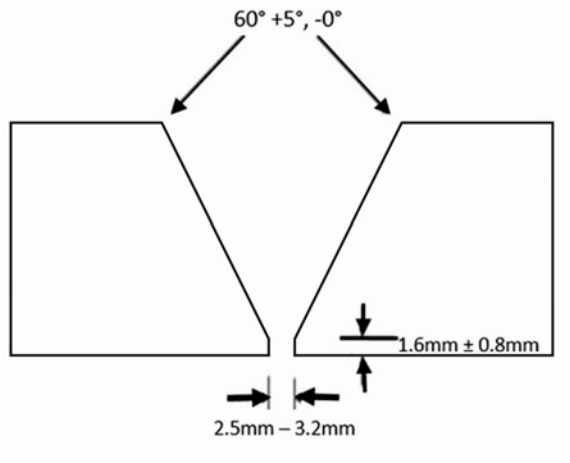

Fig. 1. Weld groove detail.

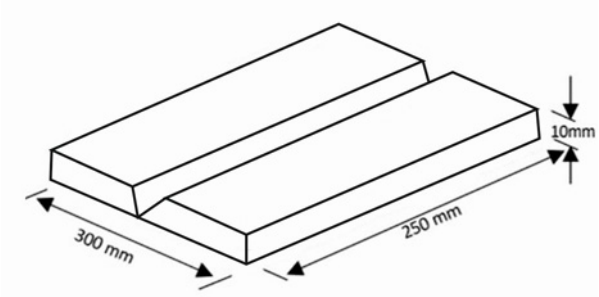

Fig. 2. PA welding position detail.

Table 2. Chemical composition (wt.%) of Magmaweld MG 3 welding wire

C	Si	Mn
0.07	0.95	1.7

currents and two different argon-carbon dioxide ratio combinations. The resulting weld joints were subjected to various tests, including tensile, bending, microhardness, macro, and microstructure analyses, to determine the effects of these factors on the weld's structure and mechanical properties. The investigations revealed that an increase in welding current and carbon dioxide ratio led to grain coarsening in both the weld metal and the heat-affected zone. Furthermore, it was found that the increase in welding current and carbon dioxide ratio increased the hardness in these regions while reducing the yield and tensile strength.

In this study, the MAG welding method was used to join S355J2 with normalized steel using a semi-automatic welding mechanism. Nine different shielding gas mixtures were tested at 3 different welding speed values. The resulting welds were subjected to hardness tests, bending tests, microstructure analysis, and SEM and EDS analyses, which were examined and discussed.

2. Experimental studies

2.1. Material and method

In this study, 15 × 25 × 1 cm^3 plates of S355J2 with normalized structural steel were used, and V-shaped weld grooves were opened using a milling cutter. The weld grooves were mutually aligned, tack welded, and made ready for welding. It was then fixed to the work table in the PA position. The weld groove detail is shown in Fig. 1, and the PA welding position detail is shown in Fig. 2. The chemical content of the S355J2 with normalized structural steel is shown in Table 1, given in weight percentage.

In the study, for the multi-pass joining of S355J2 with normalized structural steel, Magmaweld MG 3 brand 0.12 cm 15 kg MAG filler metal with the code AWS/ASME SFA-5.18 ER70S-6 (EN ISO 14341-A G46 4) was utilized. The chemical composition of the welding wire is presented in Table 2 and expressed in weight percentage (wt.%).

In the MAG welding process, 9 different gas mixtures specified in Table 3, each with a volume of 10 liters, were used. A semi-automatic welding mechanism was created, and three welding speed settings listed in Table 3 were selected according to the welding speed capability of the welding mechanism. The structural steel was joined using a Nuriş brand 500 W--WRS model, direct current (DC) MAG welding machine with 4 coarse and 10 fine gradations.

2.2. Preparation and joining of test samples for welding

The S355J2 with normalized structural steel was cut into 15 × 25 × 1 cm^3 dimensions, and 30° V-shaped grooves were created on each piece. The pieces were then aligned and made ready for weld-

Table 3. Welding gas mixtures and speeds

Gas mixture	Speeds ($m\,min^{-1}$)
93 % argon + 5 % carbon dioxide + 2 % oxygen	0.10, 0.15, 0.225
88 % argon + 10 % carbon dioxide + 2 % oxygen	0.10, 0.15, 0.225
83 % argon + 15 % carbon dioxide + 2 % oxygen	0.10, 0.15, 0.225
92 % argon + 5 % carbon dioxide + 3 % oxygen	0.10, 0.15, 0.225
87 % argon + 10 % carbon dioxide + 3 % oxygen	0.10, 0.15, 0.225
82 % argon + 15 % carbon dioxide + 3 % oxygen	0.10, 0.15, 0.225
91 % argon + 5 % carbon dioxide + 4 % oxygen	0.10, 0.15, 0.225
86 % argon + 10 % carbon dioxide + 4 % oxygen	0.10, 0.15, 0.225
81 % argon + 15 % carbon dioxide + 4 % oxygen	0.10, 0.15, 0.225

ing. The welding processes were carried out using 9 different gas mixtures and at 3 different welding speeds for each gas mixture. For welding speeds of 0.10 and 0.15 $m\,min^{-1}$, the welding process involved a root pass, a hot pass, and a cover pass. For the welding speed of 0.225 $m\,min^{-1}$, the welding process involved a root pass, a hot pass, and two cover passes. A gas mixture with a flow rate of 12 liters per minute and a wire feed speed (WFS) of 490 centimeters per minute was used. The welding processes were carried out using an average of 145 A and 18.5 V values. To examine the effects of gas in the welding processes, gas flow rates, amperage, voltage, and wire feed rates were kept constant.

2.3. Mechanical tests and metallographic examinations applied to joints

In the study, the welded test specimen was processed in CNC milling by ASTM E 190-14 standard and brought to its final dimensions for bending test. Four bending test specimens were prepared from each welded part. A Microanalysis brand Universal testing machine model device with a capacity of 100 KN was used to carry out the bending test.

In the study, fracture surfaces of samples subjected to the Charpy V-notch impact test in the weld metal region were used for EDS analysis of SEM images. In addition to these samples, polished and etched surface samples prepared for optical microscopy and SEM images for EDS analysis were also used in this study. Samples containing the base material and the weld area were determined and extracted for microstructure analysis. The samples prepared for these examinations were sanded with 60, 120, 400, 600, 800, and 1200 numbered abrasives, respectively, and then polished on a polishing cloth with alumina oxide paste. Metkon brand device was used for this process. Etching was done by holding it in 2 % Nital solution for about 3 seconds. Both the surface of the broken samples and the surface of the polished and etched samples separately 250×, 500×, 1000×, and 2000× magnified images were taken with a scanning electron microscope (SEM), and elemental analyses (EDS) were performed. TESCAN MIRA3 XMU brand and model device was used for SEM and EDS processes.

An optical microscope of the Nikon brand was utilized to examine the microstructure of the sample. Images of each sample were taken from the pass in the cap area, the HAZ regions on the right and left of the cap, the pass in the root region, the HAZ regions on the right and left sides of the root, the weld filler metal and the base metal, and 50×, 100×, and 400× magnification was made for each of these images. A total of 30 images were taken with an optical microscope. This process was carried out in the same way for 27 samples.

The hardness measurements of the welded test specimen were carried out according to the ASTM 92-82 standard from the weld filler metal, HAZ region, from the base material along the line, 15 cover passes, and 15 root passes for 30 points. Vickers hardness scans were carried out with a Shimadzu brand Vickers Hardness Tester with a load capacity of HV 0.5 kg.

3. Discussion of results

3.1. Bend test results

Four samples, two from the cap and two from the root, were subjected to three-point bending tests to determine whether the welded materials had a macro defect. Figure 3 shows the samples after the bending test.

The welding velocity-bending distribution graph for all gas mixtures is presented in Fig. 4. According to the graph, the welding sample carried out at a welding speed of 0.15 m/min, with a gas mixture of 92 % argon + 5 % carbon dioxide + 3 % oxygen and at a pressure of 1129.888 MPa, resulted in the highest bending value. The lowest bending value was obtained from 839.3175 MPa and 88 % argon + 10 % carbon dioxide + 2 % oxygen gas mixture at 0.10 $m\,min^{-1}$ welding speed. As a result of the test, no tearing or cracking

Fig. 3. View of specimens after bending test.

was generally detected, no welding faults such as cold adhesion were encountered, and the test was successfully passed.

3.2. SEM images and EDS results

SEM images of the fracture surfaces of the weld metal regions of the notch impact samples are shown in Figs. 5a, 6a, and 7a. These samples were obtained from the weld using a gas mixture of 92 % argon + 5 % carbon dioxide + 3 % oxygen, which is considered to have the best mechanical properties among all gas mixtures, at welding speeds of 0.10, 0.15, and 0.225 m min^{-1}. The images were captured at a magnification of 2000×, and EDS analysis values were also obtained. EDS analysis values were obtained and given according to the regions marked with numbers 1, 2, and 3 on the SEM images. EDS analysis values are given in Figs. 5b, 6b, and 7b. Even though an increase in the carbon dioxide content of the shielding gas resulted in a decrease in the levels of silicon and manganese elements within the weld metal, it caused an increase in the formation of oxides such as MnO and SiO_2. Although these oxides are mostly mobile and removed from the weld metal as slag, a certain amount remains within the weld metal as inclusions [12–14].

Inclusions have a spherical shape and are formed within pits. The size of the inclusions and the pits increases as the amount of carbon dioxide in the shielding gas increases. The increase in carbon dioxide during the welding process triggers various reactions, including the decomposition of carbon dioxide into oxygen and carbon monoxide within the arc. As a result, elements such as silicon, manganese, and titanium in the weld metal content decrease, increasing the number and size of inclusions within the weld metal [12, 15].

A shielding gas containing a higher proportion of argon decreases the size and distribution of inclusions within the weld metal. In addition, the inclusions en-

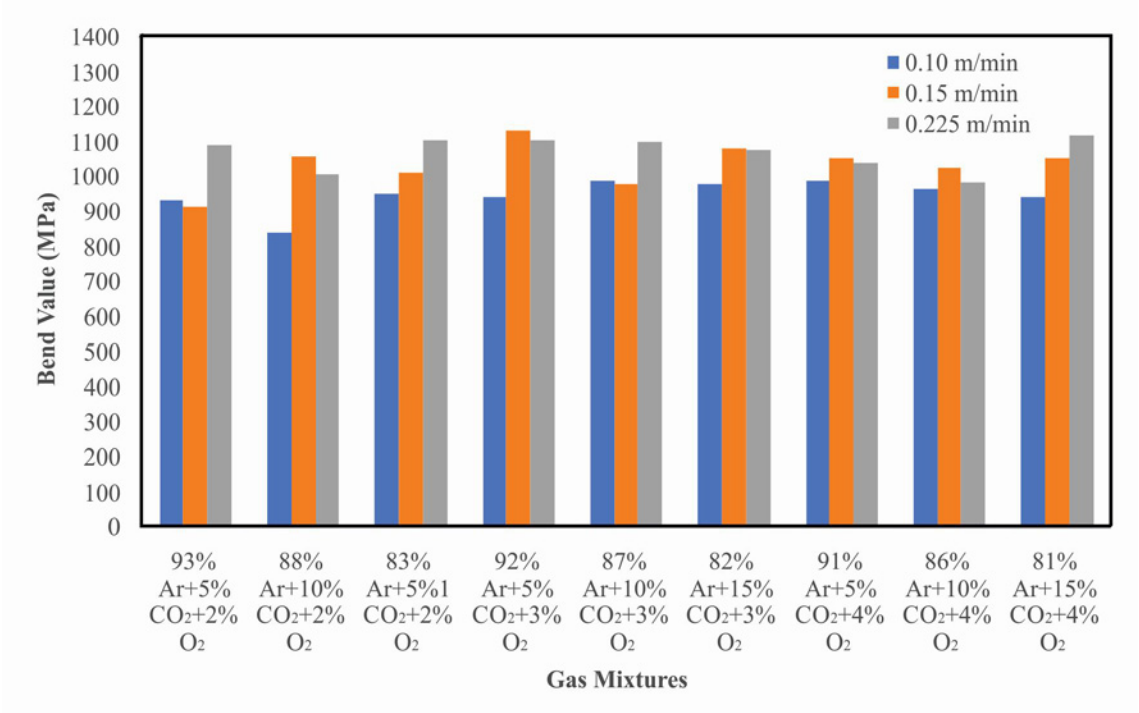

Fig. 4. Welding velocity-bending distribution graph of gas mixtures.

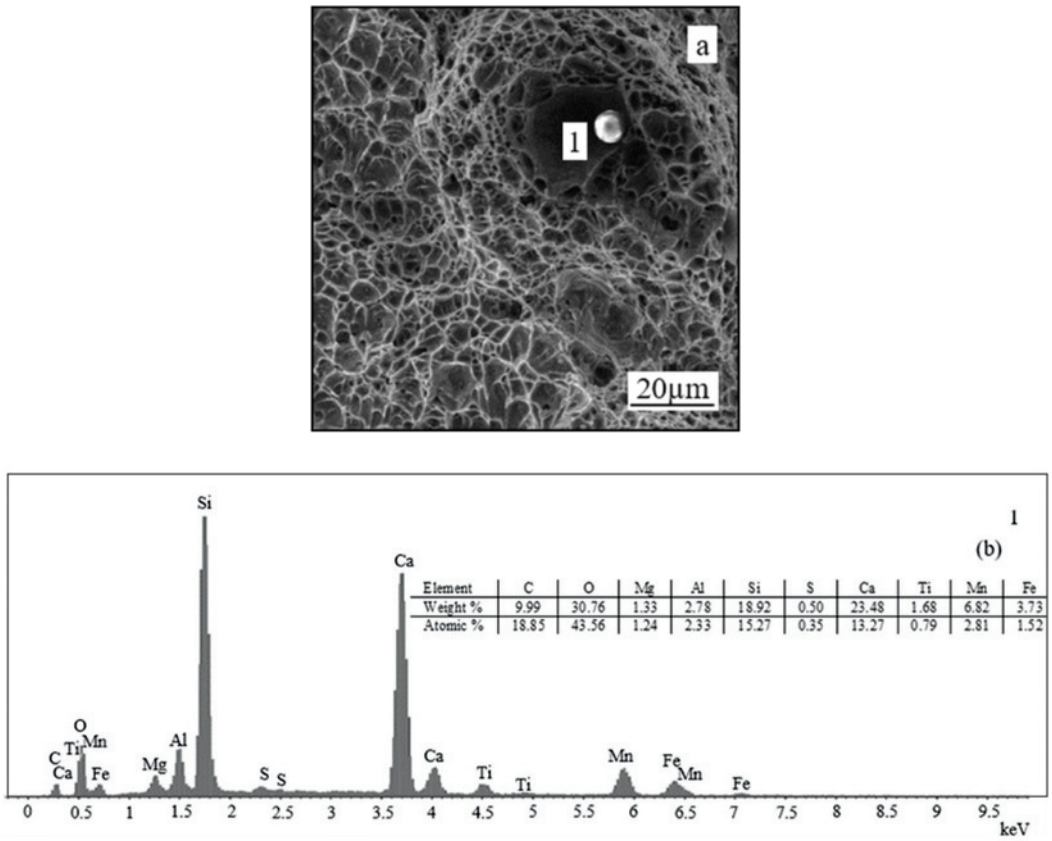

Fig. 5. (a) SEM image and (b) EDS analysis of 92 % argon + 5 % carbon dioxide + 3 % oxygen mixture at 0.10 m min^{-1}.

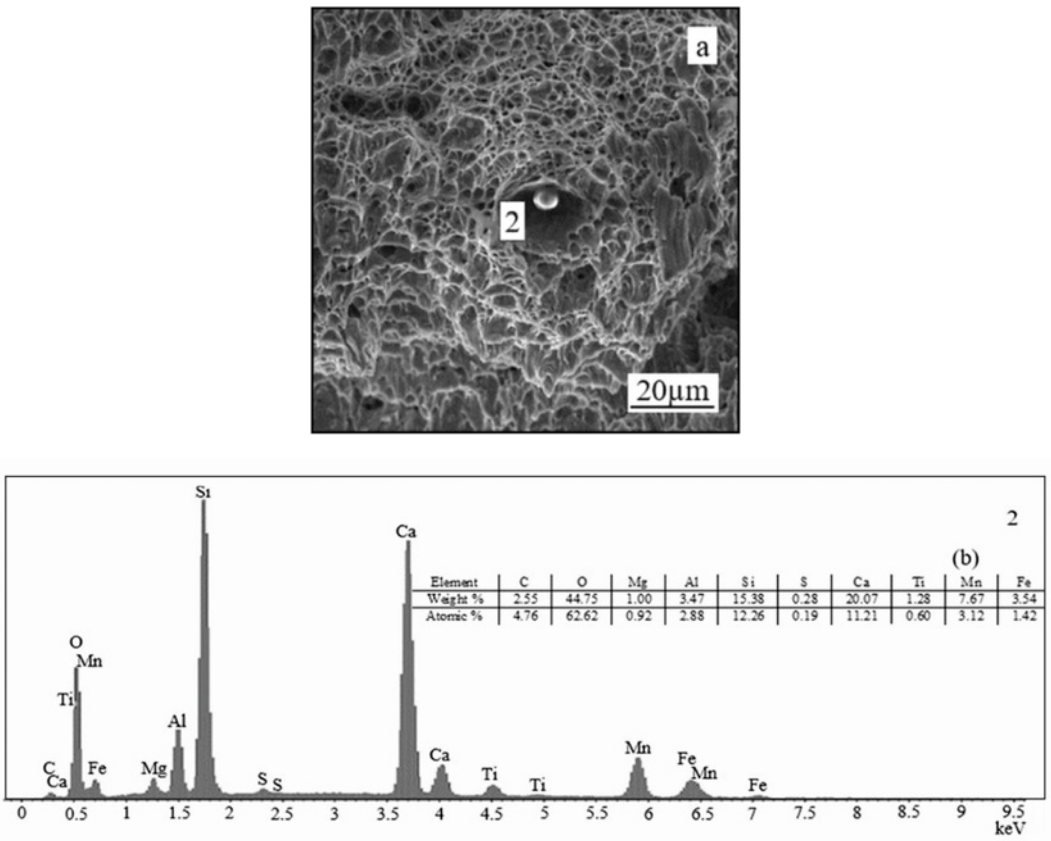

Fig. 6. (a) SEM image and (b) EDS analysis of 92 % argon + 5 % carbon dioxide + 3 % oxygen mixture at 0.15 m min^{-1}.

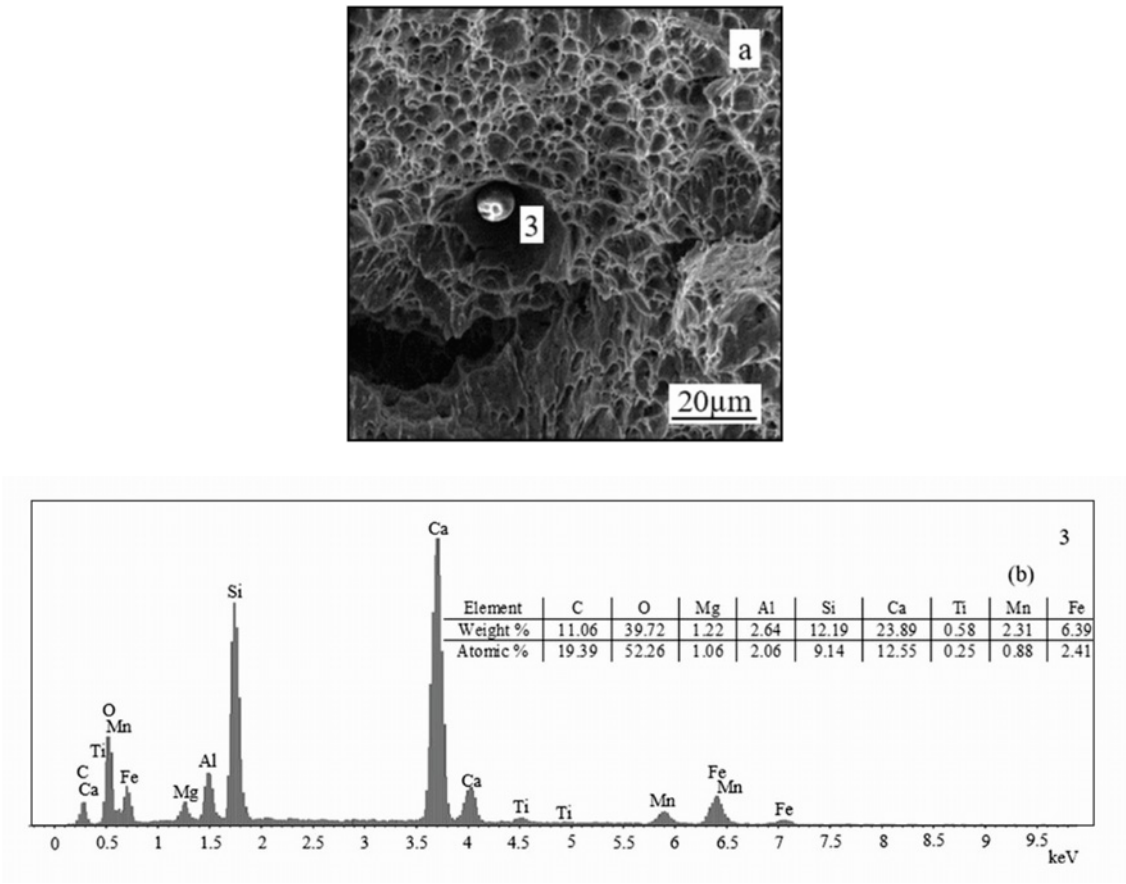

Fig. 7. (a) SEM image and (b) EDS analysis of 92 % argon + 5 % carbon dioxide + 3 % oxygen mixture at 0.225 m min^{-1}.

large the dimensions of the pits in which they are located [12–14, 16–19]. The pits containing inclusions are deeper and have gaps adjacent to the inclusions. The fracture surface morphology of the inclusions reveals flat, cleavage fracture zones [12].

The EDS analysis indicates that the inclusions are comprised of multiple oxides. The silicon and manganese within the weld metal do not function as deoxidizers above 1800 ℃, thus precipitating as microparticles [19]. The use of carbon dioxide shielding gas results in increased heat input, which in turn increases the diffusion of oxygen within the weld pool [20]. The inclusions are formed through the combination of elements with a high affinity for oxygen, such as silicon, manganese, titanium, and aluminum, resulting in the creation of multiple oxide forms.

As revealed through the EDS analysis, the increased heat within the weld pool causes the formation of inclusions within the weld metal as a result of oxygen, with those formed on the surface of the weld pool being added to the resulting slag. The inclusions probably consist of FeO, CrO, Si_2O, TiO_2, MnO, and Al_2O_3 and range in size from 1 to 8 µm [12].

In Figs. 8a,b, the SEM image of the polished and etched surface sample of the base metal prepared for optical microscopy at 2000× magnification, and the obtained EDS analysis values are given. In Figs. 9a,b, Figs. 10a,b, and Figs. 11a,b SEM images of the weld metal regions of the samples with polished and etched surfaces prepared for optical microscopy, obtained from the weld of a gas mixture of 92 % argon + 5 % carbon dioxide + 3 % oxygen gas mixture, which is thought to exhibit the best mechanical properties among all gas mixtures, at a welding speed of 0.10, 0.15, and 0.225 m min^{-1} at 2000× magnification and the obtained EDS analysis values are given. EDS analysis values are obtained from the full surface visible in the SEM images.

Based on the EDS analysis results, it was found that the ratios of silicon and manganese elements in the weld metal, obtained with different gas mixtures, as shown in Figs. 9b and 11b, were higher than the ratios in the base metal, despite a decrease due to oxidation. This is due to the additional reinforcement of silicon and manganese elements from the welding wire.

When examining the SEM images of the samples, it was observed that cracking occurred between the grains, and the structure was ductile due to the presence of small and deep micro-voids (dimples).

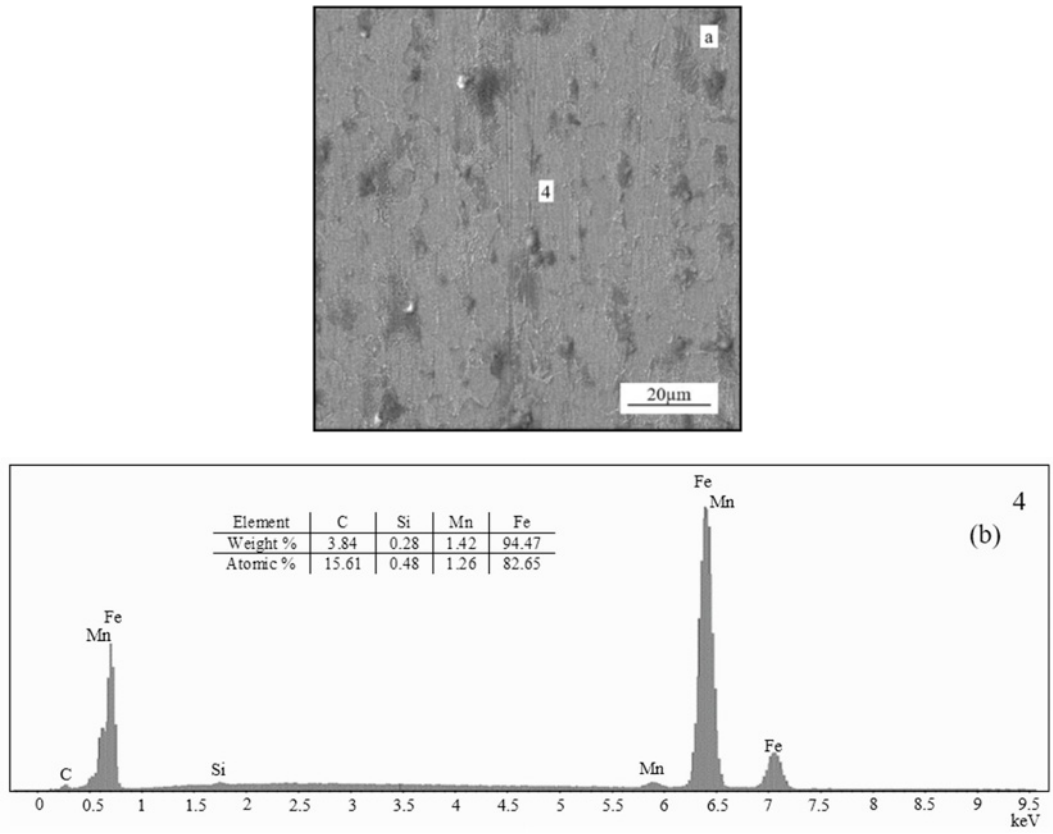

Fig. 8. (a) SEM image and (b) EDS analysis of base metal.

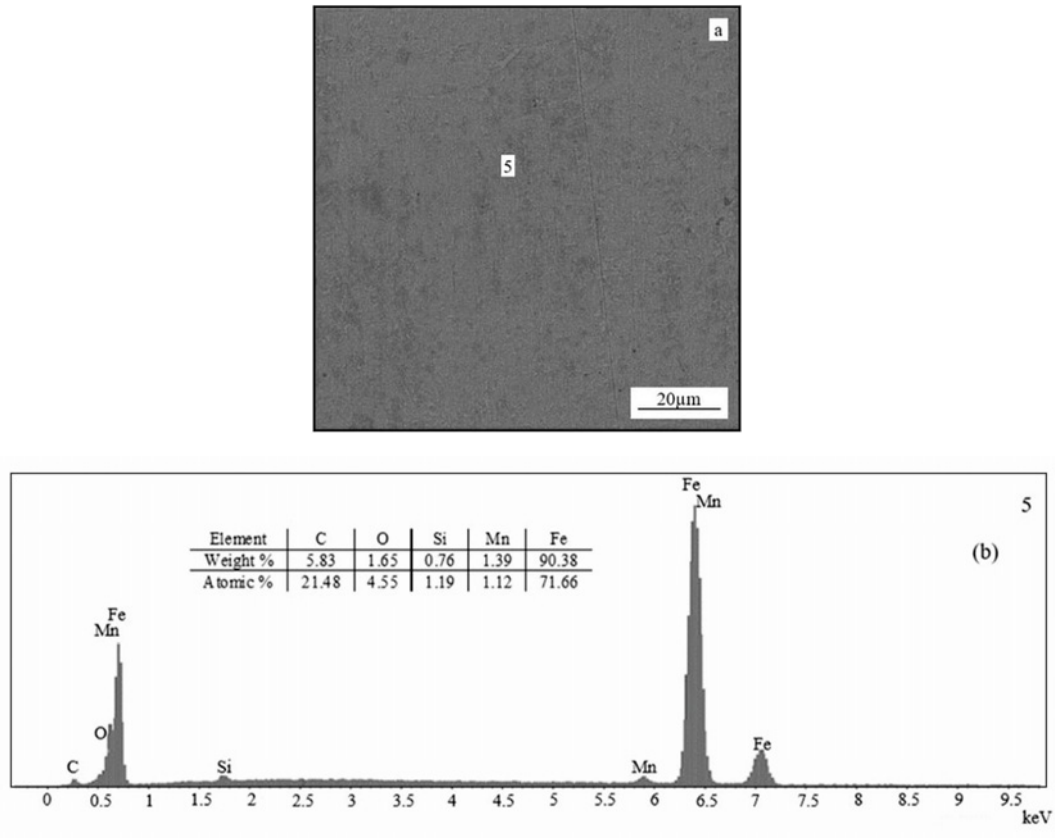

Fig. 9. (a) SEM image and (b) EDS analysis of 92 % argon + 5 % carbon dioxide + 3 % oxygen mixture at 0.10 m min^{-1}.

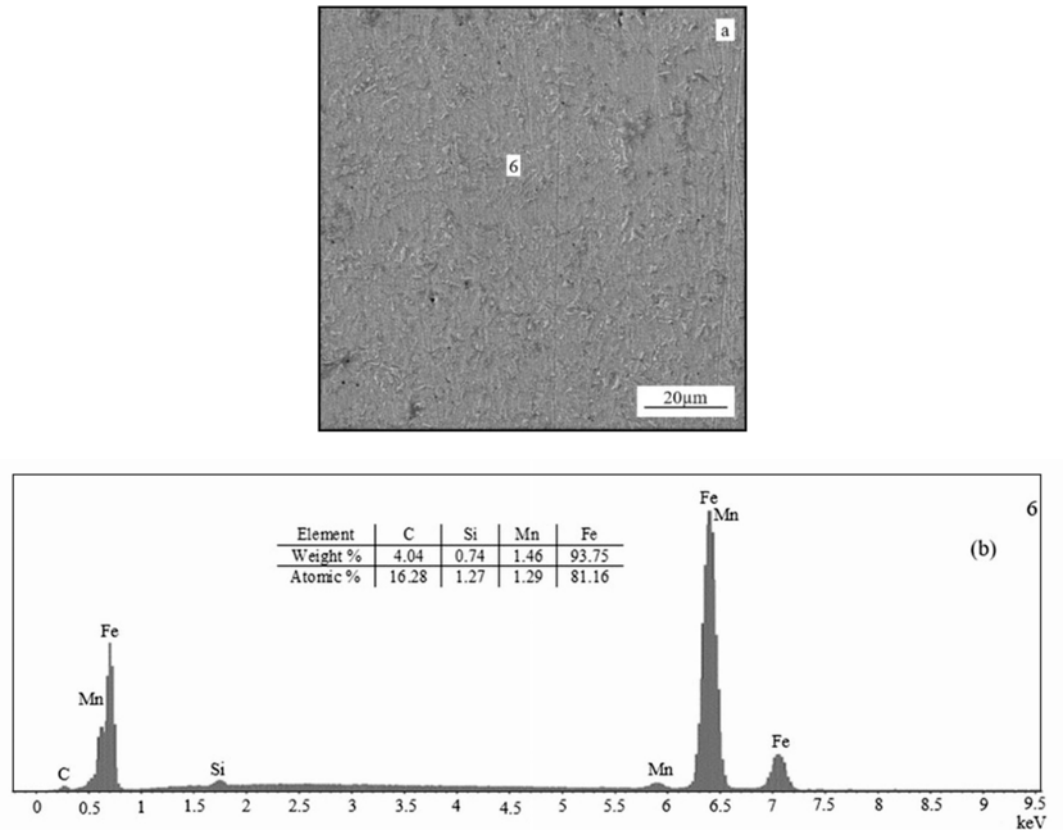

Fig. 10. (a) SEM image and (b) EDS analysis of 92 % argon + 5 % carbon dioxide + 3 % oxygen mixture at 0.15 m min^{-1}.

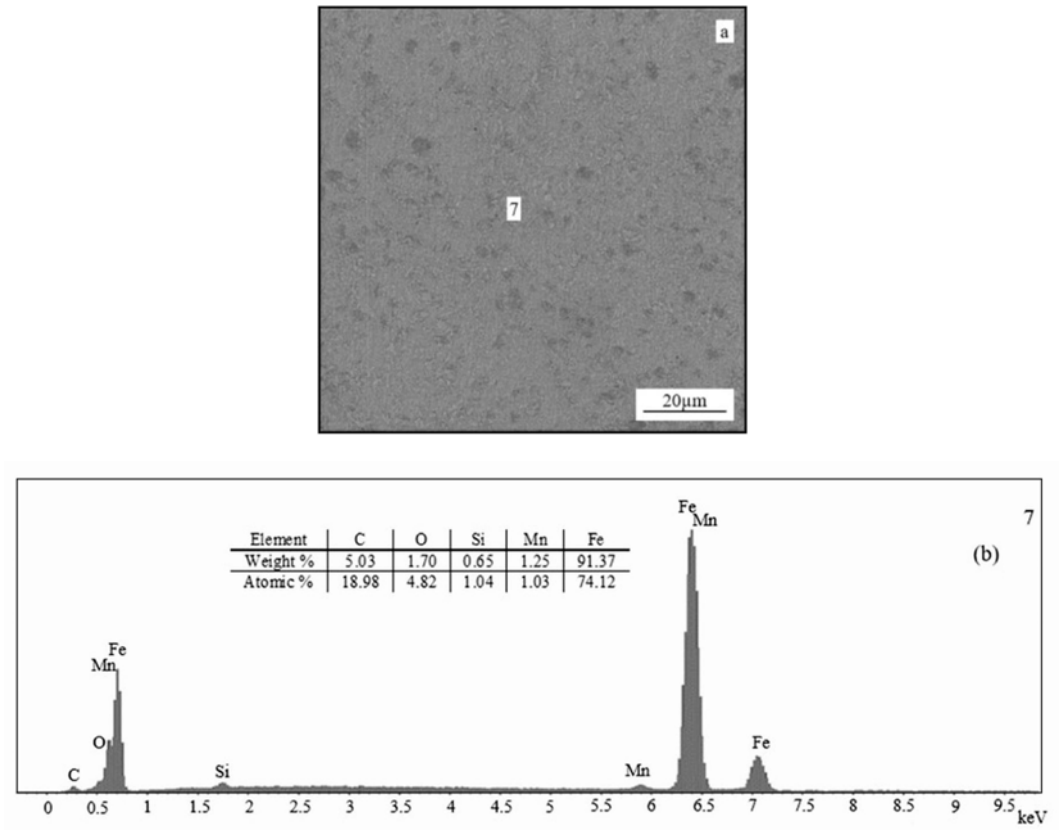

Fig. 11. (a) SEM image and (b) EDS analysis of 92 % argon + 5 % carbon dioxide + 3 % oxygen mixture at 0.225 m min^{-1}.

3.3. Hardness test results

A total of 30 hardness values obtained from the regions specified in the standard for the hardness test specimens were also applied to 27 welded specimens. The hardness values obtained due to the hardness measurements of each welded sample are shown in Figs. 12a–i.

Upon examination of the hardness charts provided for the cap and root passes, it is observed that the base metal has the lowest hardness values, while the HAZ region has the highest. Regarding the HAZ zones, the welds with the lowest welding speed of 0.10 m min^{-1} exhibit the lowest hardness values. According to the hardness values between the HAZ zones, the highest hardness values are seen in the welds with the highest welding speed, which is 0.225 m min^{-1}. This is approximately seen in the hardness values in Figs. 12a–d with low carbon dioxide and oxygen ratios. The cooling rate and the chemical composition of the base material influence the hardness of welded joints. The main factors affecting the heat input are welding speed, arc current, and arc voltage. In our experiments, if the arc voltage and current are considered constant, increasing the welding speed results in a decrease in the material's heat input and, consequently, an increase in the cooling rate of the HAZ. Since this situation causes the formation of hard phases such as fine pearlite, bainite, and martensitic structure, the hardness increases as the welding speed increases in the samples [21, 22].

The increase in carbon dioxide in the shielding gas leads to a higher plasma temperature in the arc, increasing the heat input in the weld pool [23]. The increase in heat input results in an extended cooling

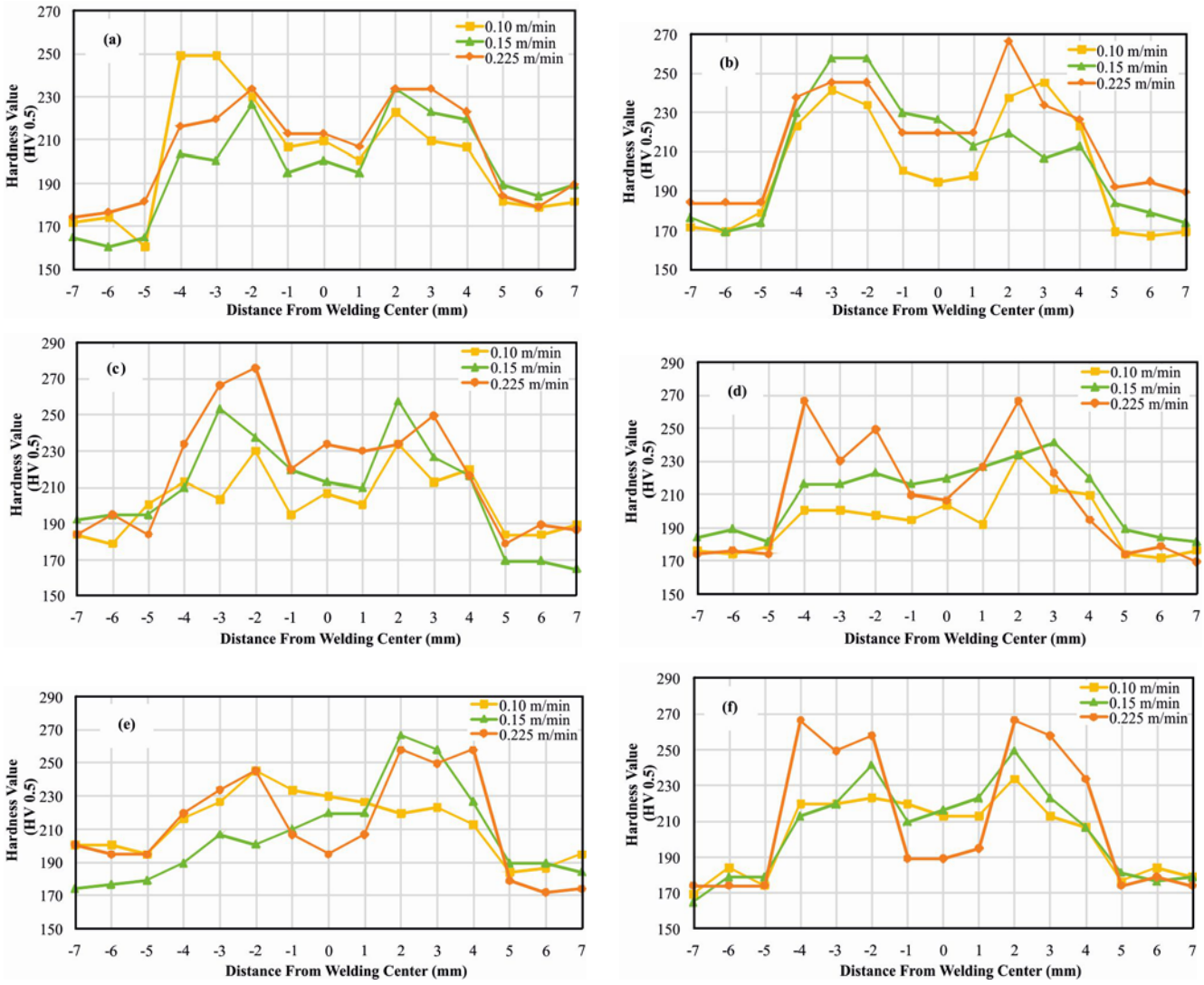

Fig. 12a–f. Hardness distribution graph of (a) 93 % argon + 5 % carbon dioxide + 2 % oxygen, (b) 88 % argon + 10 % carbon dioxide + 2 % oxygen, (c) 83 % argon + 15 % carbon dioxide + 2 % oxygen, (d) 92 % argon + 5 % carbon dioxide + 3 % oxygen, (e) 87 % argon + 10 % carbon dioxide + 3 % oxygen, and (f) 82 % argon + 15 % carbon dioxide + 3 % oxygen.

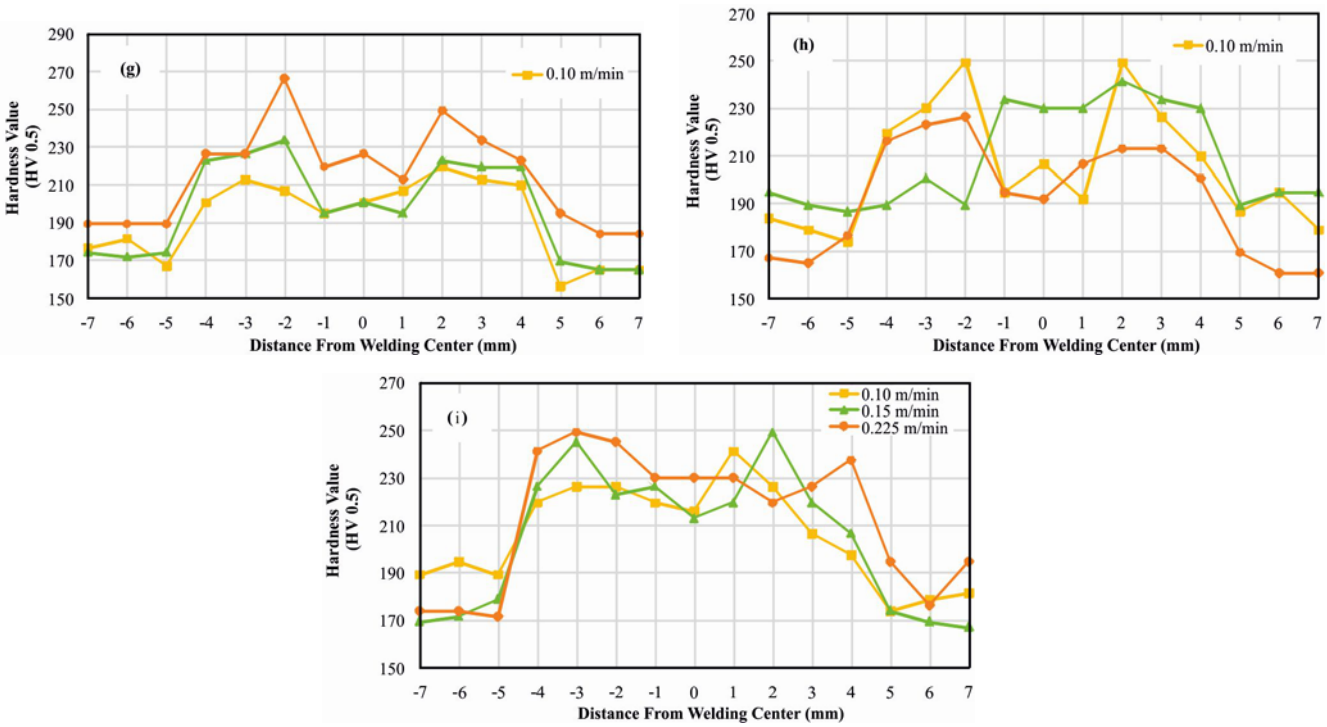

Fig. 12g–i. Hardness distribution graph of (g) 91 % argon + 5 % carbon dioxide + 4 % oxygen, (h) 86 % argon + 10 % carbon dioxide + 4 % oxygen, and (i) 81 % argon + 15 % carbon dioxide + 4 % oxygen.

time, causing a decrease in the hardness of the weld metal as the amount of carbon dioxide in the shielding gas increases.

Looking at the hardness values in Figs. 12e–i with high carbon dioxide and oxygen ratios shows the situation in Figs. 12a–d is the opposite in some parts. In other words, according to the hardness values between the HAZ regions in Figs. 12e–i, the lowest hardness values are seen in welds made at 0.225 m min^{-1} in some places, while the highest hardness values are seen in welds made at 0.10 m min^{-1} in others. This phenomenon is believed to be attributed to oxides forming from increased carbon dioxide and oxygen ratios. When the active components, namely the amounts of oxygen and carbon dioxide in the shielding gas, are high, the oxygen ratio in the weld metal also increases, leading to a decrease in the ratios of Mn and Si in the electrode [24]. Mn and Si cause an increase in mechanical properties. The presence of oxygen speeds up the formation of readily soluble oxides. To counteract the oxidizing effect of oxygen, the levels of alloying elements such as silicon, manganese, aluminum, titanium, and zirconium in the welding wire are increased [25].

3.4. Metallographic examination results

In Figs. 13a–i, 100× magnified microscope images of the ITAB regions of the samples are given.

Figures 13a–i present microstructural images of the weld metal, fusion line, and HAZ regions. One notable observation in the microstructures is the grain growth, which is influenced by the heat input in the weld metal and HAZ. Specifically, grain coarsening is only observed in the HAZ region. The changes in microstructure types and the coarse-grained internal structure lead to a decrease in hardness on the base material side of the HAZ.

The cooling rate in the HAZ is primarily determined by the heat input and the thickness of the base metal in the joint. High heat inputs cause low cooling rates in HAZ. Cooling rates in thick sections are also higher than in thin sections. Cooling rates are also affected by the temperature of the base metal before and during welding [21, 22].

Due to the density of acicular ferrite grains formed due to overheating and rapid cooling during welding, a finer-grained structure is observed in the weld metal [26, 27]. It is well-known that the formation of fine-grained structures positively affects the mechanical properties [28]. In the HAZ, it is observed that grains elongate dendritically from the base metal towards the weld metal due to the influence of heat. It has also been found that a needle-like Widmanstatten ferrite structure forms within the HAZ grain structure, where the dendritic structure is prevalent [29]. As the acicular ferrite content decreases in the samples, the hardness value in the weld zone decreases. This indicates that an increase in carbon dioxide in the shielding gas leads to decreased acicular ferrite and increased Widmanstatten ferrite [23]. This variation in the ferrite content can be ex-

plained by examining the changes in the cooling rate under different shielding gas compositions [30]. Increased carbon dioxide in the shielding gas results in longer heat input and cooling times, leading to a microstructure with fewer out-of-equilibrium phases [23].

4. Conclusions

The present study examined the influence of various shielding gas compositions and welding speeds on the welding properties of S355J2 with normalized structural steel using the MAG welding method. The

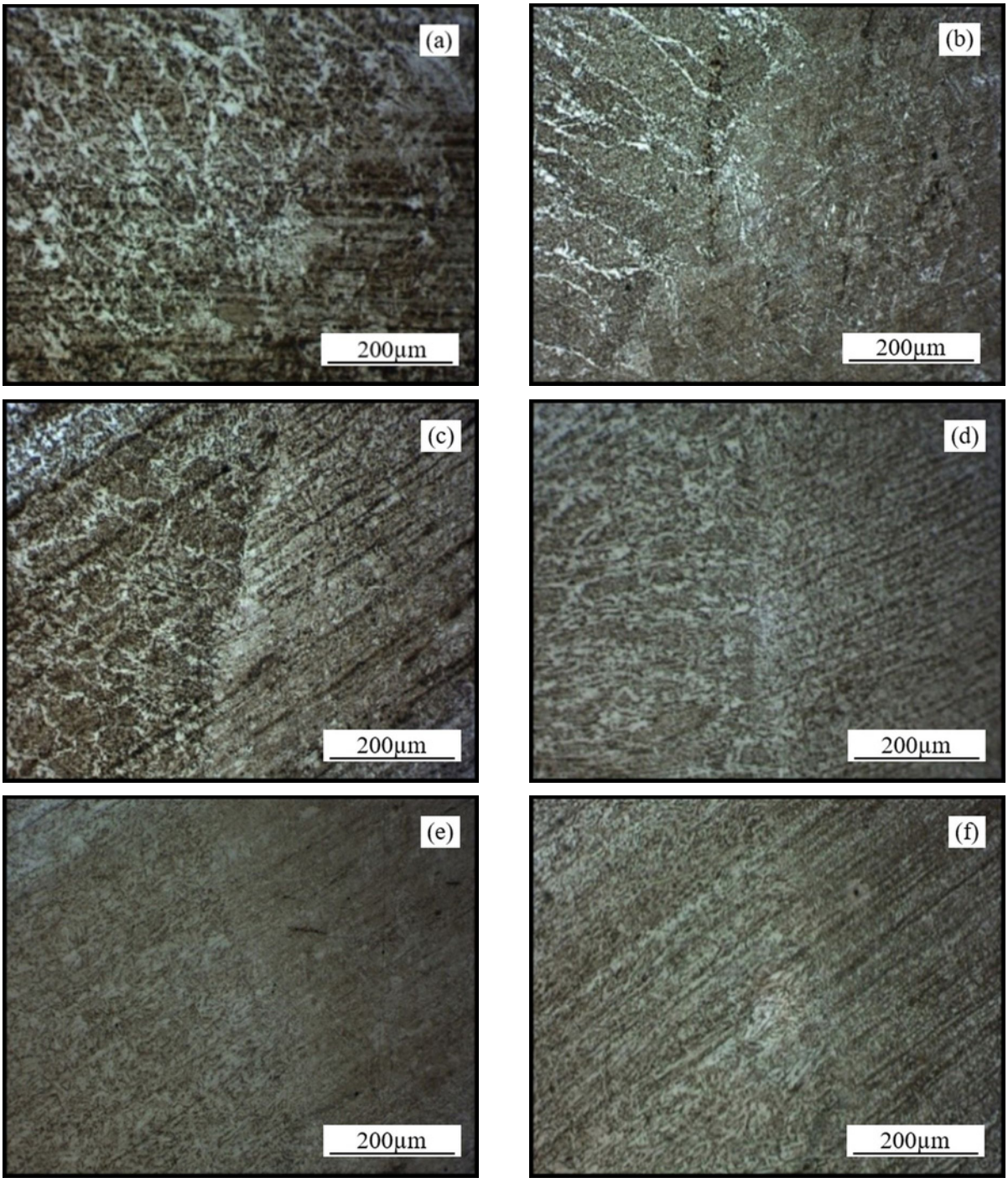

Fig. 13a–f. HAZ of (a) 93 % argon + 5 % carbon dioxide + 2 % oxygen, (b) 88 % argon + 10 % carbon dioxide + 2 % oxygen, (c) 83 % argon + 15% carbon dioxide + 2 % oxygen, (d) 92 % argon + 5 % carbon dioxide + 3 % oxygen, (e) 87 % argon + 10 % carbon dioxide + 3 % oxygen, and (f) 82 % argon + 15 % carbon dioxide + 3 % oxygen.

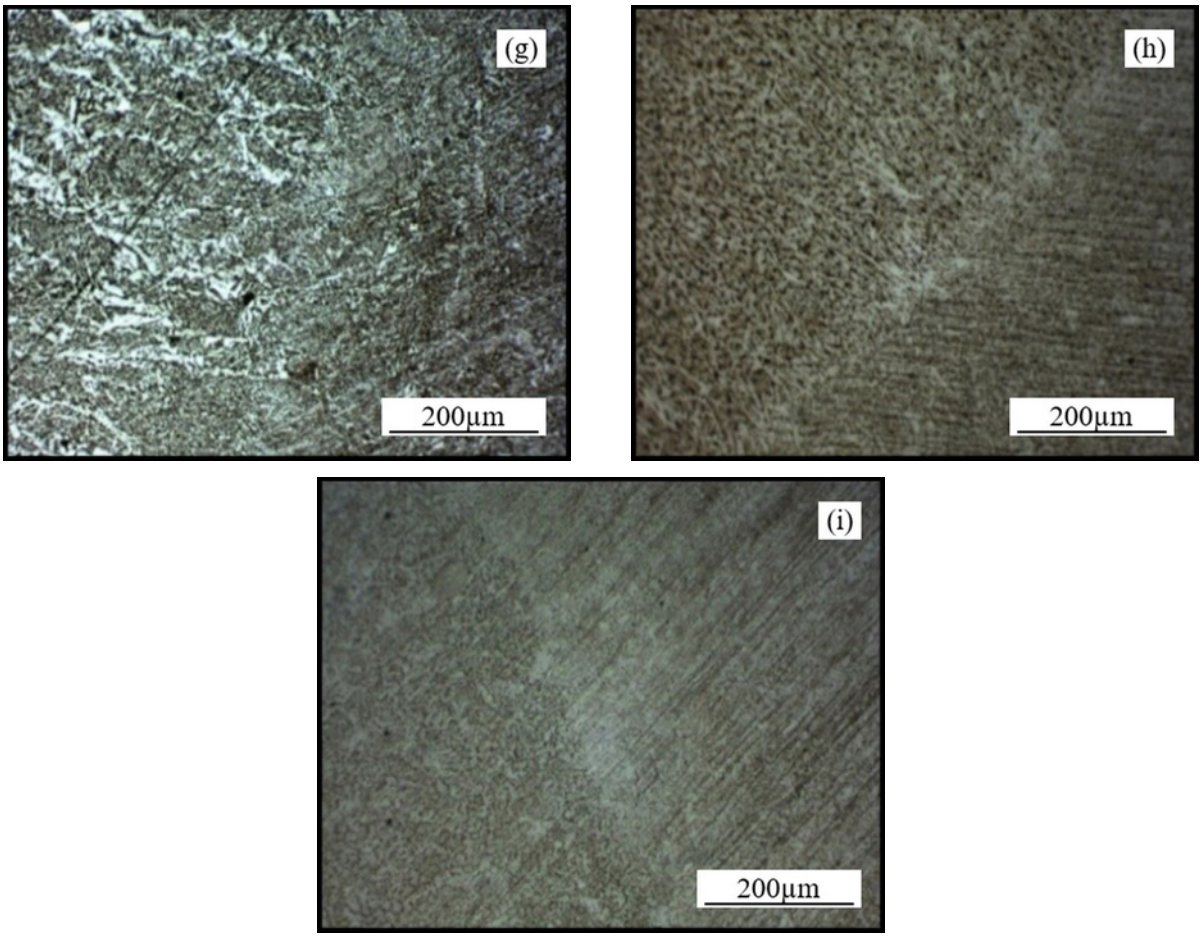

Fig. 13g–i. HAZ of (g) 91 % argon + 5 % carbon dioxide + 4 % oxygen, (h) 86 % argon + 10 % carbon dioxide + 4 % oxygen, and (i) 81 % argon + 15 % carbon dioxide + 4 % oxygen at 0.15 m min^{-1}.

experimental analysis included bending tests, SEM and EDS examinations, microstructural analysis, and hardness testing. The findings are summarized as follows:

1. The welding sample with the highest bending value was obtained using a gas mixture of 92 % argon + 5 % carbon dioxide + 3 % oxygen at a welding speed of 0.15 m min^{-1}, while the lowest bending value was observed in the sample welded at a welding speed of 0.10 m min^{-1} using a gas mixture of 88 % argon + 10 % carbon dioxide + 2 % oxygen.

2. The bending test revealed no tearing or cracking, and defects such as cold adhesion were not observed in the welded samples.

3. Under the influence of increased heat input, carbon dioxide can decompose in the arc to release oxygen and carbon monoxide, which increases oxygen diffusion in the weld pool. The increase in carbon dioxide in the shielding gas reduced silicon and manganese elements in the weld metal. However, it also combined with elements with a high affinity for oxygen, such as silicon and manganese, resulting in increased oxides like MnO and SiO_2. Some of these oxides remained as inclusions in the weld metal, increasing the number and size of inclusions in it.

4. EDS analysis revealed that increased heat in the weld pool results in oxygen-induced inclusions in the weld metal.

5. Using shielding gas with a higher percentage of argon reduces the size and distribution of inclusions in the weld metal.

6. According to the EDS analysis results, while the silicon and manganese ratios decreased due to oxidation, it was observed that they were higher in the weld metal than in the base metal due to the additional reinforcement of silicon and manganese elements from the welding wire when comparing the ratios of general silicon and manganese elements in the base metal with those in the weld metal obtained with different gas mixtures.

7. As the welding speed increases, the material heat input decreases, and therefore, the cooling rate of the HAZ increases, which increases the hardness.

8. The hardness of the weld metal decreases as the amount of carbon dioxide in the shielding gas composition increases, increasing the heat input and, there-

fore, the cooling time.

9. An increase in oxygen and carbon dioxide ratios in the shielding gas leads to an increase in the oxygen ratio in the weld metal, which affects the hardness values due to oxidation.

10. Grain coarsening is observed to occur only in the weld metal-associated region. Hardness decrease is observed on the main material side of HAZ due to the coarse-grained internal structure.

11. The hardness value in the weld zone decreases as the content of acicular ferrite decreases in the samples.

12. It can be concluded that an increase in the amount of carbon dioxide in the shielding gas leads to a decrease in the amount of acicular ferrite and an increase in the amount of Widmanstatten ferrite.

References

[1] H. Ada, S. Aksöz, T. Fındık, C. Çetinkaya, B. Bostan, B. İ. Candan, The investigation of effect of welding process on the microstructure and mechanical properties of API 5L X65 Steel welded with Gas Metal Arc Welding Method, Çukurova University Journal of the Faculty of Engineering and Architecture 31 (2016) 1–9. https://doi.org/10.21605/cukurovaummfd.311031

[2] M. G. Çınar, V. Onar, H. Efe, Microstructure analysis of xar steel plate welded by mag welding method using different welding currents, International Journal on Mathematic, Engineering and Natural Science 3 (2019) 123–130.

[3] S. Anık, Kaynak Tekniği El Kitabi, Gedik Holding Yayımı, İstanbul, 1991.

[4] E. R. Pierre, Shielding Gases For Welding, Welding Design&Fabrication, USA, 1987.

[5] F. Raoufi, Parameter Optimization in MIG/MAG Welding Processes, METU Metallurgical and Materials Engineering. [Master's Thesis] Ankara, 1994.

[6] J. Kuna, Effect of shielding gas mixture on the impact toughness of pulsed arc welded joints, Technical University of Wroclaw, Poland, 1989.

[7] L. E. Svensson, Control of Microstructures and Properties In Steel Arc Welds, CRC Press, USA, 1994.

[8] A. Şık, The effect of shielding gas mixture on tensile strength of MIG/MAG welded Construction Steel (St52-3), Trakya Univ. J. Sci. 7 (2006) 9–15.

[9] M. Türk, A. Demirer, The effect of shielding gas and welding groove on mechanical properties in joining surface hardened S355J0 Steel welded by GMAW, European Journal of Science and Technology 32 (2021) 392–397. https://doi.org/10.31590/ejosat.1042314

[10] D. Avisans, I. Boiko, A. Avisane, Influence of 8 % CO_2 and argon shielding gas mixture on MAG welding of high strength steel (650 MPa) in spray arc, International Scientific Conference Engineering For Rural Development, Jelgava (2022), pp. 936–942. https://doi.org/10.22616/ERDev.2022.21.TF295

[11] Y. Kargın, F. Çavdar, E. Kanca, Investigation on effects of current and protective gas combination in MAG welding of S460MC Structural Steel, Journal of Characterization 2 (2022) 176–184. https://doi.org/10.29228/JCHAR.64011

[12] R. Yılmaz, M. Tümer, Microstructural studies and impact toughness of dissimilar weldments between AISI 316 L and AH36 steels by FCAW, Int J Adv Manuf Technol. 67 (2013) 1433–1447. https://doi.org/10.1007/s00170-012-4579-0

[13] M. T. Liao, W. J. Chen, The effect of shielding gas compositions on the microstructure and mechanical properties of stainless steel weldments, Materials Chemistry and Physics 55 (1998) 145–151. https://doi.org/10.1016/S0254-0584(98)00134-5

[14] B. Arivazhagan, S. Sundaresan, M. Kamaraj, A study on influence of shielding gas composition on toughness of flux-cored arc weld of modified 9Cr–1Mo (P91) steel, Journal of Materials Processing Technology 209 (2009) 5245–5253. https://doi.org/10.1016/j.jmatprotec.2009.02.006

[15] J. Norrish, Advanced Welding Processes, Springer Science & Business Media (2006) pp. 82–25. ISBN 9781845691301

[16] M. T. Liao, W. J. Chen, A comparison of gas Metal Arc Welding with Flux-Cored Wires and Solid Wires using shielding gas, Int J Adv Manuf Technol. 15 (1999) 49–53. https://doi.org/10.1007/s001700050038

[17] D. Katherasan, P. Sathiya, A. Raja, Shielding gas effects on flux cored arc welding of AISI 316L (N) austenitic stainless steel joints, Materials and Design 45 (2013) 43–51. https://doi.org/10.1016/j.matdes.2012.09.012

[18] R. Yılmaz, M. Tümer, The Effect of Shielding Gases on the Microstructure and Toughness of Stainless Steels Weldments by FCAW, 63. Annual Assembly & International Conference of the International Institute of Welding, (2010), pp. 847–852, Istanbul.

[19] S. Mukhopadhyay, T. K. Pal, Effect of shielding gas mixture on gas metal arc welding of HSLA steel using solid and flux-cored wires, Int J Adv Manuf Technol. 29 (2006) 262–268. https://doi.org/10.1007/s00170-005-2510-7

[20] L. Shanping, F. Hidetoshi, N. Kiyoshi, Effect of CO_2 shielding gas additions and welding speed on GTA weld shape, Journal of Materials Science 40 (2005) 2481–2485. https://doi.org/10.1007/s10853-005-1979-7

[21] G. Türkkan, The effect of gas flow rate on weld penetration and welding speed in shielding gas welding (MIG/MAG), Dokuz Eylul University Institute of Science and Technology [Master Thesis] İzmir, 2008.

[22] L. M. Gourd, Principles of Welding Technology, Hodder Arnold 1986. ISBN-10: 0713136022.

[23] M. Ebrahimnia, M. Goodarzi, M. Nouri, M. Sheikhi, Study of the effect of shielding gas composition on the mechanical weld properties of steel ST 37-2 in gas metal arc welding, Materials and Design 30 (2009) 3891–3895. https://doi.org/10.1016/j.matdes.2009.03.031

[24] V. Balraj, K. L. Rohira, Evaluation of shielding gas and flux composition effects on weld bead properties, Int. J. For The Joining of Materials 4 (1992).

[25] T. Kurşun, The effect of shielding gas and gas mixtures used in gas arc welding technique on the mechanical properties of 19Mn6 quality steel in welding and

comparison with submerged arc welding, Erciyes University Institute of Science, [Master Thesis] Kayseri, 1998.
[26] S. Shanmugam, R. D. K. Misra, J. Hartmann, S. G. Jansto, Microstructure of high strength niobium containing pipeline steel, Materials Science and Engineering A 441 (2006) 215–229. https://doi.org/10.1016/j.msea.2006.08.017
[27] S. H. Hashemi, D. Mohammadyani, Characterisation of weldment hardness, impact energy and microstructure in API X65 steel, International Journal of Pressure Vessels and Piping 98 (2012) 8–15. https://doi.org/10.1016/j.ijpvp.2012.05.011
[28] P. Lehto, H. Remes, T. Saukkonen, H. Hänninen, J. Romanoff, Influence of grain size distribution on the Hall–Petch relationship of welded structural steel, Materials Science and Engineering A 592 (2014) 28–39. https://doi.org/10.1016/j.msea.2013.10.094
[29] K. Easterling, Introduction to the Physical Metallurgy of Welding, Butterworth-Heinemann, England, 1992.
[30] J. F. Lancaster, Metallurgy of Welding, London: Chapman & Hall (1976) 122–35.